1

Effect of Control Constraints on Active Stabilization of Flutter

K.S. Vikhorev ⋆, M.G. Goman ⋆⋆, M.N. Demenkov ⋆⋆⋆

The University of Nottingham, Nottingam, NG8 1BB, UK
De Montfort University, Leicester, LE1 9BH, UK

Summary. The effect of amplitude and rate control constraints in active flutter suppression is analysed for a number of different state feedback control laws considering mathematical model of two degree-of freedom nonlinear aeroelastic airfoil system with trailing and leading edge flaps. The size of region of attraction is used as an additional metric to select a set of acceptable control laws designed by eigenstructure assignment and nonlinear dynamic inversion methods.

1 Introduction

Different control techniques have been successfully applied for suppression of flutter instability of BACTM (Benchmark Active Control Technology Model) and nonlinear wing section model in wind tunnel experiments [8, 10, 9, 12, 2]. However, in all these studies the problem of control constraints and their effect on the size of region of attraction was not clearly presented. The qualitative investigation of the closed-loop dynamics for nonlinear wing section model is presented in [6]. In this paper stabilization of flutter instability of nonlinear wing section system [9] is investigated with saturated state feedback control laws designed by eigenstructure assignment and nonlinear dynamic inversion (NDI) methods. The size of the closed-loop system stability region is evaluated by computation of critical magnitudes

⋆ PhD Student, School of Computer Science and IT, Faculty of Science, e-mail: kxv@cs.nott.ac.uk
⋆⋆ Professor, Faculty of Computing Science and Engineering, e-mail: mgoman@dmu.ac.uk
⋆⋆⋆ Research Fellow, Faculty of Computing Science and Engineering, e-mail: demenkov@dmu.ac.uk

of state variables leading to instability. The continuation of Limit-Cycle Oscillations (LCO) using MATCONT package [11] and computation of non-local stability maps illustrate effect of deflection limit and rate saturation on the size of stability region.

2 Wing Section Mathematical model

The equations of motion of nonlinear aeroelastic wing section system (see Fig. 1a) have the following form [9]:

$$\begin{bmatrix} m_T & m_W x_\alpha b \\ m_W x_\alpha b & I_\alpha \end{bmatrix} \begin{vmatrix} \ddot{h} \\ \ddot{\alpha} \end{vmatrix} + \begin{bmatrix} c_h & 0 \\ 0 & c_\alpha \end{bmatrix} \begin{vmatrix} \dot{h} \\ \dot{\alpha} \end{vmatrix} + \begin{bmatrix} k_h & 0 \\ 0 & k_\alpha(\alpha) \end{bmatrix} \begin{vmatrix} h \\ \alpha \end{vmatrix} = \begin{vmatrix} -L(t) \\ M(t) \end{vmatrix} \quad (1)$$

$$L = \rho U^2 b s C_{l_\alpha} \left[\alpha + (\dot{h}/U) + \left(\frac{1}{2} - a \right) b(\dot{\alpha}/U) \right] + \rho U^2 b s C_{l_\beta} \beta + \rho U^2 b s C_{l_\gamma} \gamma$$

$$M = \rho U^2 b^2 s C_{m_{\alpha-eff}} \left[\alpha + (\dot{h}/U) + \left(\frac{1}{2} - a \right) b(\dot{\alpha}/U) \right] + \\ + \rho U^2 b^2 s C_{m_{\beta-eff}} \beta + \rho U^2 b^2 s C_{m_{\gamma-eff}} \gamma \quad (2)$$

where α, h are the pitch angle and the plunge displacement, L and M are the quasi-steady aerodynamic force and moment, respectively, U is the flow speed, β, γ are the trailing- and leading-edge flap control deflections, $k_\alpha(\alpha) = k_0 + k_1\alpha + k_2\alpha^2$ is the stiffness coefficient nonlinearly dependent on the pitch angle, all parameters representing mass, geometry, stiffness and aerodynamic characteristics of the wing section system are taken from [9]. Equations (1) and (2) can be represented in a compact vector form:

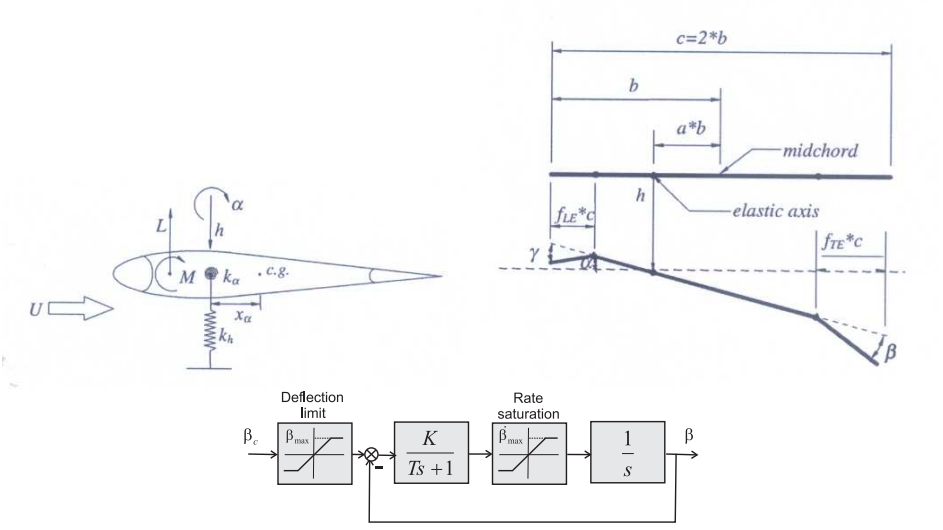

Fig. 1 The wing section model (a). The actuator model: deflection and rate saturation constraints (b).

$$M\ddot{x} + D\dot{x} + K(\alpha)x = Cu \tag{3}$$

where $x = (h, \alpha)^T$, $u = (\beta, \gamma)^T$ and matrices M,D,K and C can be found in [6]. Transformed to the Cauchy form equations (3) have the following state-space representation:

$$\begin{bmatrix} \dot{x} \\ \dot{y} \end{bmatrix} = \begin{bmatrix} 0_{2,2} & I_{2,2} \\ -M^{-1}K(\alpha) & -M^{-1}B \end{bmatrix} \begin{bmatrix} x \\ y \end{bmatrix} + \begin{bmatrix} 0_{2,2} \\ M^{-1}C \end{bmatrix} \begin{bmatrix} \beta \\ \gamma \end{bmatrix} \tag{4}$$

where $y = (\dot{\alpha}, \dot{h})^T$, $0_{2,2}$ and $I_{2,2}$ are second order zero and identical matrices, respectively.

The leading- and trailing-edge flaps can be actuated by servomotors, as in [3, 9], or hydraulic actuators, which both have physical limitations on rate and amplitude of deflection. For example, the aeroelastic apparatus in the Texas A&M University [3] has the following deflection and rate constraints $|\beta|, |\gamma| < 15$ deg. $|\dot{\beta}|, |\dot{\gamma}| < 273$ deg/s (4.75 rad/s). These constraints, represented by saturation functions in actuator model shown in Fig. 1b, do not affect local dynamics in the closed-loop system, but can produce significant changes in closed-loop dynamics at large amplitudes due to saturation of control effectors. We will consider a state feedback control law:

$$\begin{bmatrix} \beta_c \\ \gamma_c \end{bmatrix} = A_c x + B_c y + G_c(x) \tag{5}$$

where gain matrices matrices A_c and B_c are specified by eigenstructure assignment method and vector function G_c compensates system (3) nonlinearities when the leading- and trailing-edge flaps are used simultaneously. For example, the following nonlinear dynamic inversion (NDI) control law linearizes and simultaneously decouples the system dynamics in the case of unsaturated control deflections:

$$\begin{gathered} A_c = -C^{-1}MK_*; \qquad B_c = C^{-1}(D - MD_*); \qquad G_c(x) = C^{-1}K(\alpha)x \\ D_* = \begin{bmatrix} 2\xi_h\omega_h & 0 \\ 0 & 2\xi_\alpha\omega_\alpha \end{bmatrix}; \qquad K_* = \begin{bmatrix} \omega_h^2 & 0 \\ 0 & \omega_\alpha^2 \end{bmatrix}; \qquad \ddot{x} + D_*\dot{x} + K_*(\alpha)x = 0 \end{gathered} \tag{6}$$

Gain matrices A_c and B_c in (5) can be also designed using the robust pole assignment method [5] applied for the linearised system (3), when $k_1 = k_2 = 0$. This control law optimizes the choice of eigenvectors so that they minimize the sensitivity of the closed-loop poles to perturbations of the linearised system matrices. The robust pole assignment algorithm is implemented in Matlab as function *place*. This linear state feedback control law can be used with and without nonlinear compensation function $G_c(x)$.

3 Computation of non-local stability maps

State feedback control law (5) guarantees stabilization of flutter instability only locally. Due to saturation of control effectors the region of attraction of a stabilized equilibrium may be bounded and its size can vary significantly. The closed-loop cycle or additional equilibria existing in the closed-loop system (see [6]) will attract dynamics after action of disturbances exceeding their critical level. The region of attraction as a nonlocal characteristic of control law (5) depends both on feedback matrices A_c, B_c, stiffness nonlinearity k_2, k_3 and control constraint parameters $\beta_{max}, \dot{\beta}_{max}$ ($\gamma_{max}, \dot{\gamma}_{max}$).

To simplify search of stabilizing control laws (5) which maximize stability region we will use several design scenarios for eigenstructure assignment. The first scenario #1 for pole placement implies that two stable open-loop eigenvalues will remain unchained $\lambda_{1,2}^{cl} = \lambda_{st}^{ol}$ and two unstable ones are placed in different points of selected region in the left half of the complex plane $\lambda_{3,4}^{cl} = \varsigma \pm j\omega$, where $\varsigma \in (-15, 0), \omega \in (0, 15)$. This scenario stems from the property of sub-optimal control law for trailing-edge flap, which provides practically maximum region of attraction under action of only deflection limit. This linear state-feedback control law can be obtained using the LQR design when $J = \int_0^\infty u^T(t)u(t)dt$ [4, 1, 7]. In terms of pole placement the sub-optimal control law leaves unchanged two stable open-loop eigenvalues and reflects to the stable half of the complex plane two unstable eigenvalues, i.e. they change only sign of their real parts. Rate constraints $\dot{\beta}_{max}, \dot{\gamma}_{max}$ and stiffness nonlinearities ($k_2 \neq 0; k_3 \neq 0$) will affect this optimality condition. To find out corrected feedback matrices in (5) maximizing the size of stability region under action of both constraints and nonlinear stiffness the proposed scenario provides freedom in pole placement of unstable eigenvalues.

The second scenario #2 for closed-loop pole placement implies that two identical complex conjugate pairs are placed in different points of specified region in the left-half of the complex plane $\lambda_{1-4}^{cl} = \varsigma \pm j\omega$, where $\varsigma \in (-15, 0), \omega \in (0, 15)$. For leading- and trailing-edge flaps there is an additional freedom for choice of closed-loop eigenvectors. Another two scenarios will be used to define them. The first one will use the robust pole placement [5], implemented by Matlab function *place*, and the second one will decouple the pitch and plunge airfoil motion as implemented in (6).

The control law (5) designed locally considering different scenarios for eigenstructure assignment is validated in this paper by estimation of its region of attraction. This involves simulation of dynamic processes under action of large amplitude disturbances which lead to control saturation. For every design point the size of region of attraction is evaluated by computing critical disturbances α_{cr} and h_{cr} (see Fig. 2), which belong to the boundary of region of attraction. The isolines α_{cr} or h_{cr} are plotted in the considered design region of pole placement (for example, see Fig. 3 and 4). The maps of isolines α_{cr} or h_{cr} reflect non-local

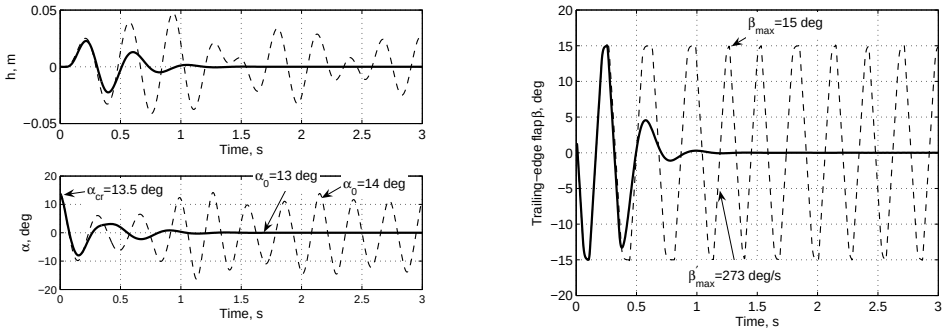

Fig. 2 Critical disturbance in pitch angle α_{cr} (convergence to stabilized equilibrium or to large amplitude oscillations with saturated control).

stability properties of locally designed control law (5), so we will call them as Non-Local Stability Maps (NLSMs).

4 Computational examples

Nonlocal stability maps (NLSMs) presented in this section for several design scenarios provide control law design solutions which can be acceptable for flutter stabilization including conditions with large level of external disturbances. Continuation of periodical oscillations (LCO) and analysis of their multipliers using MATCONT package [11] shed light on the nature of significant enlargement of region of attraction at the best design conditions.

4.1 Trailing-Edge Flap

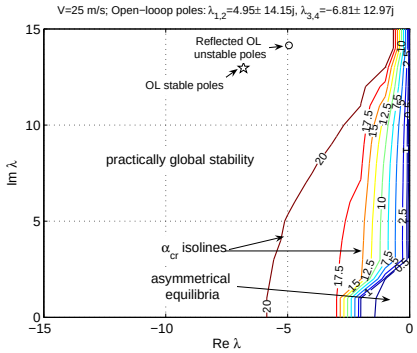

Fig. 3 Nonlocal stability map for α_{max}. Pole placement scenario #1, trailing-edge flap without rate constraints $\dot{\beta}_{max} = \infty$.

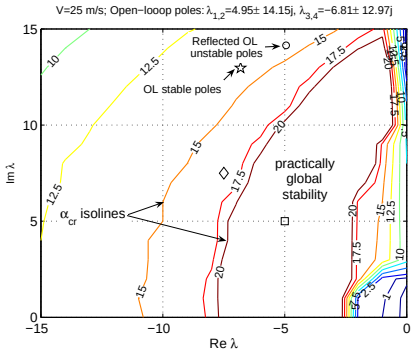

Fig. 4 Nonlocal stability map for α_{max}. Pole placement scenario #1, trailing-edge flap with rate constraint $\dot{\beta}_{max} = 273$ deg/s.

The NLSMs presented in Figs. 3 and 4 demonstrate that the aeroelastic wing section model can be effectively stabilized using only the trailing-edge flap control. The NLSM in Fig. 3 corresponds to the sub-optimal control law [1, 7] and does not take into account rate saturation effect ($\dot{\beta}_{max} = \infty$). The NLSM in Fig. 4 is computed for the same control law with account of rate saturation when $\dot{\beta}_{max} = 273$ deg/s (this rate constraint is taken from [3]). Isolines in these two figures separate pole placement regions which are characterized by different level of critical disturbances α_{cr} (NB: the isoline level changes from one degree to twenty degrees with increment $\Delta\alpha_{cr} = 2.5$ deg).

Critical disturbance α_{cr} for sub-optimal control law with pole placement, shown by star and circle markers in Figs. 3 and 4, drops significantly when $\dot{\beta}_{max} = 273$ deg/s. Placement of open-loop unstable eigenvalues across the selected part of stable half of the complex plane reveals pole placement regions with very high critical disturbances $\alpha_{cr} \gg 20$ deg. The effect of rate saturation leads to a significant decrease and relocation of the broad region with practically global stability shown in Fig. 3 (see [6]). However, the NLSM in Fig. 4 shows that

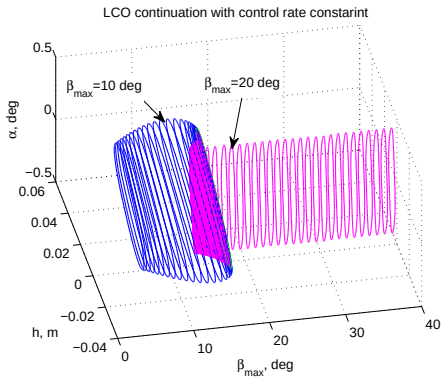

Fig. 5 LCO continuation vs maximum control amplitude at pole placement $\lambda^{cl}_{3,4} = -7.5 \pm 7.5j$.

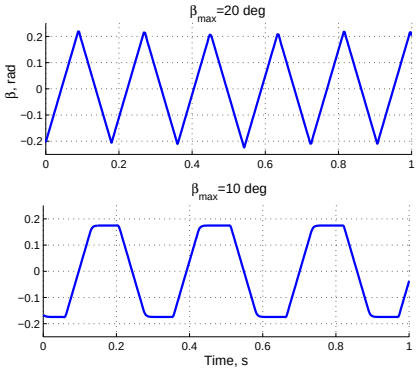

Fig. 6 Transition between two types of control saturation.

even with rate saturation the acceptable design region is still big enough for a proper selection of control law. Fig. 5 presents results of the closed-loop LCO continuation with increase of β_{max} at design point $\lambda^{cl}_{3,4} = -7.5 \pm 7.5j$ (diamond marker in Fig. 4). The closed-loop LCO, stable at $\beta_{max} < 16$ deg, after two saddle-node bifurcations is transformed to slightly unstable LCO which is surrounded by stable toroidal attractor. The LCO transformation leads to the change in character of control constraints from the tooth-type to the saw-type (see Fig. 6). The critical disturbance at this design point $\alpha_{cr} = 16$ deg. The continuation of the closed-loop LCO vs amplitude β_{max} at another design point $\lambda^{cl}_{3,4} = -5 \pm 5j$ (square marker in Fig. 4) is presented in Fig. 7 with associated multipliers shown in Fig. 8. At $\beta_{max} = 7.67$ deg the LCO becomes highly oscillatory unstable as the complex conjugate pair multipliers travel far outside from the unit circle (Fig. 8). In this case the LCO is destabilized and the toroidal attractor exists only in the close vicinity of the Neimark-Sacker bifurcation (see [6]). As a result the region of attraction in the selected design point becomes practically global.

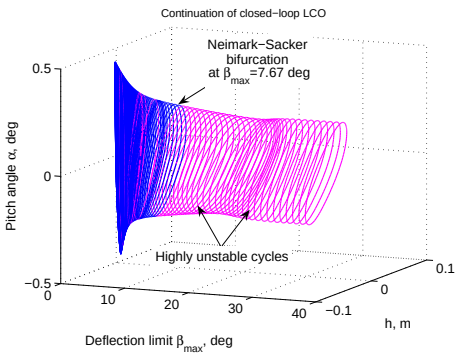

Fig. 7 LCO continuation vs maximum control amplitude at pole placement $\lambda^{cl}_{3,4} = -5 \pm 5j$.

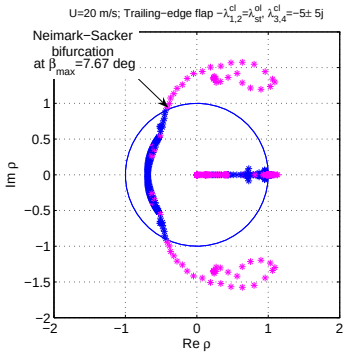

Fig. 8 Closed-loop LCO multipliers.

4.2 Trailing- and Leading-Edge Flaps

Figs. 9 - 12 show computed NLSMs for flutter stabilization using the leading- and trailing-edge flaps simultaneously. Pole placement scenario #1 is used in the first two examples and pole placement scenario #2 is used in the second two examples. Figs. 9 and 11 correspond to the case when the eigenvectors are decoupled accordingly with (6). Figs. 10 and 12 correspond to the case when the eigenvectors are assigned using Matlab *place* command providing parameteric robustness properties. There is no difference between decoupling and robust assignment when pole placement scenario #2 is applied. Example in Fig.12 includes also nonlinear dynamic inversion (NDI) accordingly to (6).

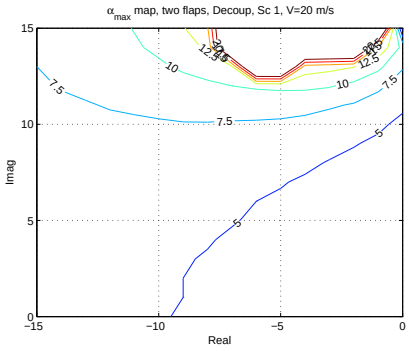

Fig. 9 Nonlocal stability map α_{max} for two flaps. Pole placement scenario #1, decoupled assignment, rate constraint $\dot{\beta}_{max} = 273$ deg/s.

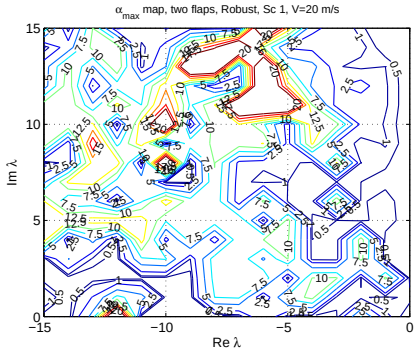

Fig. 10 Nonlocal stability map α_{max} for two flaps. Pole placement scenario #1, robust assignment, rate constraint $\dot{\beta}_{max} = 273$ deg/s.

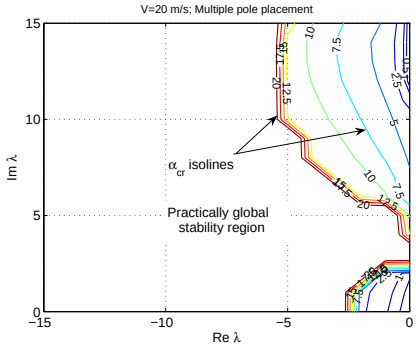

Fig. 11 Nonlocal stability map α_{max} for two flaps. Pole placement scenario #2, decoupled and robust assignment, rate constraint $\dot{\beta}_{max} = 273$ deg/s.

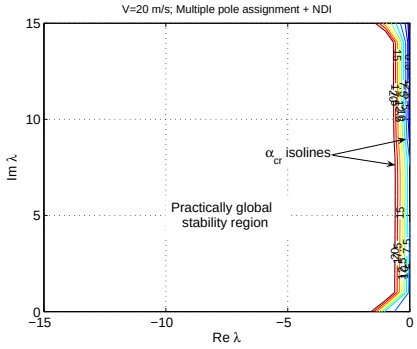

Fig. 12 Nonlocal stability map α_{max} for two flaps. Pole placement scenario #2, decoupled and robust assignment + NDI, rate constraint $\dot{\beta}_{max} = 273$ deg/s.

The presented results clearly show that in flutter stabilization using two flaps scenario #2 for pole placement is much better, the decoupling and the robust eigenvector assignment work equally well for scenario #2 and additional application of NDI improve the control law design significantly (see Fig. 12).

5 Conclusion

Flutter of the nonlinear aeroelastic wing section system with actuator constraints can be effectively stabilized under action of large external disturbances using only the trailing-edge flap. The broad region for pole placement of the open-loop unstable eigenvalues in this case has been identified when stable eigenvalues remain unchanged. The best control law design for simultaneous use of the leading- and trailing-edge flaps for flutter stabilization requires the multiple pole placement and additional nonlinear dynamic compensation of system nonlinearities.

References

1. E. Applebaum and J.Z. Ben-Asher. Control of an aeroelastic system with actuator saturation. *Journal of Guidance, Control, and Dynamics*, 30(2):548–556, 2007.
2. Franco Bernelli-Zazzera, Paolo Mantegazza, Giovanni Mazzoni, and Matteo Rendina. Active flutter suppression using recurrent neural networks. *Journal of Guidance, Control, And Dynamics*, 23(6):1030–1036, 2000.
3. Jeffrey J. Block and Thomas W. Strganac. Applied active control for a nonlinear aeroelastic structure. *Journal of Guidance, Control, and Dynamics*, 21(6):838–845, 1998.
4. T. Hu and Z. Lin. *Control systems with actuator saturation: analysis and design*. Birkhauser, Boston, 2001.
5. J. Kautsky and N.K. Nichols. Robust pole assignment in linear state feedback. *Int. Journal of Control*, 41, 1985.
6. M.G.Goman and M.N.Demenkov. Multiple attractor dynamics in active flutter suppresssion problem. *ICNPAA 2008: Mathematical Problems in Engineering, Aerospace and Sciences*, Genoa, Italy 2008.
7. M.N.Demenkov and M.G.Goman. Suppressing aeroelastic vibrations via stability region maximization and numerical continuation techniques. *UKACC International Control Conference*, Manchester 2008.
8. Vivek Mukhopadhyay. Transonic flutter suppression control law design and wind-tunnel test results. *Journal of Guidance, Control, and Dynamics*, 23(5):930–937, 2000.
9. George Platanitis and Thomas W. Straganac. Control of a nonlinear wing section using leading- and trailing-edge surfaces. *Journal of Guidance, Control, And Dynamics*, 27(1):52–58, 2004.
10. Martin R.Waszak. Robust multivariable flutter suppression for benchmark active control technology wind-tunnel model. *Journal of Guidance, Control, and Dynamics*, 24(1):147–153, 2001.
11. A. Dhooge W. Govaerts and Y.A. Kuznetsov. Matcont: a matlab package for numerical bifurcation of odes. *ACM Transactions on Mathematical Software*, 29:141–164, 2003.
12. Wen Hong Xing and Sahjendra N. Singh. Adaptive output feedback control of a nonlinear aeroelastic structure. *Journal of Guidance, Control, And Dynamics*, 23(6):1109–1116, 2000.